Development of non-local neoclassical transport code for helical configurations

Shinsuke Satake[1)], Ryutaro Kanno[1,2)] and Hideo Sugama[1,2)]

[1)] *National Institute for Fusion Science,322-6 Oroshi-cho, Toki 509-5292,, Japan*

[2)] *Department of Fusion Science, Graduate University for Advanced Studies, Toki 509-5292, Japan*

The progress in 3-dimensional, non-local neoclassical transport simulation code "FORTEC-3D" is described. The main purpose of the code is to solve the drift-kinetic equation in general 3-dimensional configuration using the δf Monte-Carlo method, and to calculate neoclassical fluxes and the time evolution of the ambipolar radial electric field simultaneously. In this article, we explain the new numerical schemes adopted for FORTEC-3D in order to overcome problems happened especially in the cases where the bifurcation of radial electric field occurs. Examples of test simulation for a LHD magnetic field configuration with bifurcated electric field are also shown. With improved numerical schemes, FORTEC-3D can calculate neoclassical fluxes and trace the time evolution stably as long as several ion collision times, which is long enough to observe GAM damping and transition of the ambipolar electric field.

Keywords: neoclassical transport, δf Monte-Carlo method, ambipolar radial electric field

1 Introduction

Detailed calculation of neoclassical transport in 3-dimensional configuration plasmas such as LHD is important for transport analysis, since in a 3-dimensional system the ambipolar condition $\Gamma_i(\rho,E) = \Gamma_e(\rho,E)$ determines the radial electric field profile $E(\rho)$, where Γ_i and Γ_e are ion and electron particle fluxes across the flux surface $\rho = const$. It is known that the ambipolar condition is mainly determined by neoclassical transport. If the ambipolar condition has multiple roots, bifurcation of radial electric field profile occurs.[1] In LHD plasmas, appearance of positive electric field, or the "electron root", is preferable since it reduces neoclassical transport compared with that in negative one, or the "ion root".[2] Moreover, strong sheared electric field profile at the bifurcation point is generally considered to be favorable from the viewpoint of suppression of anomalous transport.

Neoclassical transport theory for 3-dimensional helical configuration[3, 4] has been constructed under the assumption of local transport model where the typical orbit width in the minor-radius direction is assumed to be negligible compared with the background gradient scale lengths of a plasma. Recently non-local effects, or finite-orbit-width (FOW) effects, on neoclassical transport have attracted attention in the analysis of core transport in tokamaks, where particle orbits with large widths break the assumption of conventional neoclassical theory.[5, 6] In helical configurations, the deeply ripple-trapped and transition particles show large deviation in radial direction. The FOW effect of these orbits will be important in neoclassical transport analysis if the collisionality becomes quite low. The presence of strong-sheared electric field will also brings the non-local effect to neoclassical transport. However, the applicability of analytic neoclassical theory to these situations is questionable since it neglects the FOW effect from the beginning.

From the considerations above, we have been developing a simulation code to solve the drift-kinetic equation (DKE) including the FOW effect in 3-dimensional configuration. The simulation code, FORTEC-3D,[7, 8] uses the δf Monte-Carlo method[9, 10] which has been applied to some other transport codes both for tokamaks[11] and for helical configurations.[12, 13] The features of FORTEC-3D are : (1) It uses a conserved-form linearized Fokker-Planck collision operator. (2) It is a global simulation. The entire confinement region is solved at once. (3) Time evolution of radial electric field is solved simultaneously. The ambipolar electric field is then determined in consistency with neoclassical fluxes. (4) To reduce calculation time, only the ion transport is solved by the δf method, and electron transport is solved by GSRAKE code[14] which solves bounce-averaged DKE. Note that GSRAKE solution does not include the FOW effect, and then only the non-local effect for ions transport is treated in FORTEC-3D.

So far, FORTEC-3D has successfully applied for LHD configurations to solve the formation of ambipolar field for ion roots,[7] and to study the configuration dependence of GAM oscillation and damping[8]. However, from several test calculations we found that it was difficult to apply FORTEC-3D to the cases with electron roots, since bifurcated radial electric field profile became unphysical shape as shown later. We also found that numerical noise in particle flux and numerical error in collision operator were in-

author's e-mail: satake@nifs.ac.jp

tolerably large, which had not found in tokamak cases. We ascertained the cause of these problems were from inaccuracy in radial grids for evaluating flux and electric field, and from the emergence of huge-weight markers.

In this paper, improvements for numerical schemes in FORTEC-3D recently applied to overcome the problems above are explained. In section 2, basic equations for δf Monte-Carlo method are reviewed. In section 3, modification to collision operator is described. The new operator has good conservation property with less marker numbers. In section 4, improvement in the evaluation of flux and electric field are explained. Adoption of staggered-mesh in radial direction to evaluate these two quantities makes it possible to simulate the formation of bifurcated radial electric field profile stably. In section 5, new filtering scheme for marker weights to reduce numerical noise is introduced. By comparing several tests with varied strength of filters, it is shown that the filtering scheme does not affect the solutions. By these improvements, now FORTEC-3D is ready to solve neoclassical transport in helical plasmas in varied profiles and simulate evolution of electric field including bifurcations.

2 Basic equations of the δf method

In the δf method, time development of the perturbation of plasma distribution function from the local Maxwellian $\delta f = f - f_M$ is solved according to the DKE

$$\begin{aligned} \frac{D\delta f}{Dt} &\equiv \frac{\partial \delta f}{\partial t} + \left(\mathbf{v}_\parallel + \mathbf{v}_d\right)\cdot\nabla\delta f - C_{tp}(\delta f) \\ &= -\mathbf{v}_d\cdot\nabla f_M + \mathscr{P} f_M, \end{aligned} \tag{1}$$

where C_{tp} and $\mathscr{P}$ are test-particle and field-particle parts of linearized collision operator. The magnetic field is given in the Boozer coordinate system (ψ,θ,ζ)[15] as $\mathbf{B} = \nabla\psi\times\nabla\theta + \iota\nabla\zeta\times\nabla\psi$. Practically, we use ρ for a normalized radial coordinate defined from toroidal flux ψ as $\rho = \sqrt{\psi/\psi_{out}}$. A MHD equilibrium magnetic field is constructed from the VMEC code[16]. The time evolution of radial electric field $\mathbf{E} = -d\Phi/d\rho\nabla\rho = E_\rho\nabla\rho$ is solved from the following equation

$$\varepsilon_0\varepsilon_\perp\frac{\partial E_\rho}{\partial t} = -e\left[z_i\Gamma_i - \Gamma_e\right], \tag{2}$$

where subscripts i and e describe particle species, and $\varepsilon_\perp \equiv \left[\left\langle|\nabla\rho|^2\right\rangle + \left\langle c^2|\nabla\rho|^2\right\rangle/v_A^2\right]$.

To solve eq. (1), two weights, w and p, are introduced which satisfy the relations $wg = \delta f$ and $pg = f_M$, respectively, where g is 5-dimensional simulation marker distribution function. Since the time evolution of marker distribution is given by $Dg/Dt = 0$, we obtain

$$\frac{dw}{dt} = \frac{p}{f_M}\left[-\mathbf{v}_d\cdot\nabla + \mathscr{P}\right] f_M, \tag{3a}$$

$$\frac{dp}{dt} = \frac{p}{f_M}\mathbf{v}_d\cdot\nabla f_M. \tag{3b}$$

The numerical procedures for the collision operator and for eq. (2) are described in the following sections.

3 Collision operator

The linearized Fokker-Planck operator in FORTEC-3D is made to satisfy the following relations,

$$\int d^3v\mathscr{M}\left(C_{tp}(\delta f) + \mathscr{P} f_M\right) = 0 \text{ for } \mathscr{M} = \{1, v_\parallel, v^2\}, \tag{4}$$

$$C_{tp}(\delta f) + \mathscr{P} f_M = 0 \text{ for } \delta f = (c_0 + \mathbf{c}_1\cdot\mathbf{v} + c_2 v^2) f_M. \tag{5}$$

The test-particle operator C_{tp} is expressed by random scattering in the $(v_\parallel, v_\perp)$-space. The field-particle operator is given as follows

$$\begin{aligned} \mathscr{P} &= a\left[1 - 3\sqrt{\frac{\pi}{2}}(\phi - \phi')x^{-1/2}\right]\delta n \\ &+ bv_\parallel x^{-3/2}\phi\,\delta P + cx^{-1/2}(\phi - \phi')\delta E, \end{aligned} \tag{6}$$

where $x \equiv v^2/v_{th}^2$, $\phi(x)$ is the error function, and

$$\{\delta n, \delta P, \delta E\} = \int d^3v\left\{1, v_\parallel, v^2\right\} C_{tp}(\delta f) \tag{7}$$

are changes in constants-of-motions by C_{tp} only. Previously, the relation (3b) has been used to determine constants $(a,b,c) = (1/n, 2/nv_{th}, 2/3nv_{th})$. However, it was found that the numerical error in the conservation low (4) became larger as the numerical noise $f_M - pg$ became larger. The numerical error is significant in 3-D helical configuration cases compared with 2-D cases, because in 3-D cases it is difficult to keep enough marker population in a unit volume as in 2-D cases, and the marker distribution g is distorted in the velocity space in the presence of ripple-trapped particles. In the improved version, we do not use (3b) any more to make $\mathscr{P} f_M$, but the factors (a,b,c) are determined at every moment of collision so that the conservation low is strictly satisfied. In fig. 1, the residual relative error in momentum and energy arisen at one operation of $C_{tp} + \mathscr{P} f_M$ are compared between old and new $\mathscr{P} f_M$ for several tests with varied marker numbers. For previous operator, the numerical error is larger for fewer marker case. However, the error in new operator is just the rounding-error level even in the 1600-markers calculation. We have also confirmed the other property of collision operator (5) is also kept in the new operator.

4 Radial meshes

The relation between neoclassical fluxes and radial electric field (2) is solved on discrete meshes in the ρ-coordinate. Γ_i is evaluated by the volume averaged value between i-th and $i+1$-th meshes as follows

$$\begin{aligned} \Gamma_i(\rho_{i+\frac{1}{2}}) &= \frac{1}{\Delta V_{i+1/2}}\int_{\Delta V_{i+1/2}} d^3x\int d^3v\dot{\rho}\,\delta f \\ &= \frac{1}{\Delta V_{i+1/2}}\sum_{\{k|\rho_i\le\rho_k<\rho_{i+1}\}} w_k\dot{\rho}_k C(\rho_k, i), \end{aligned} \tag{8}$$

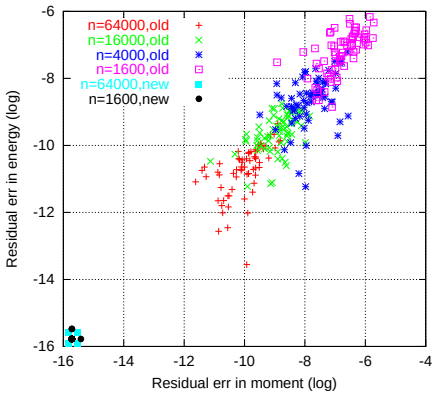

Fig. 1 Relative error in momentum and energy in one operation of $C_{tp}+\mathscr{P}f_M$. The time interval for the operation is taken $\Delta t = 2\times10^{-3}\tau_{ii}$.

where k is the marker index, and $C(\rho_k,i)$ is a shaping factor of a marker.[17] For electron flux GSRAKE solution is referred to : $\Gamma_e(\rho_{i+1/2}) = \Gamma_e(\rho_{i+1/2}, E_\rho(\rho_{i+1/2},t))^{\mathbf{GSRAKE}}$. Previously, the electric field and fluxes were evaluated on the same points $\rho=\rho_{i+1/2}$ according to eq. (2). It is illustrated in Fig. 2. However, using this scheme, we found that the electric field profile fell into an unphysical shape as shown in Fig. 3, where multiple roots for ambipolar condition are expected from GSRAKE solutions. This is because all three values in eq. (2) were evaluated on the same position, that is, the evaluation was relied on a local information too much. Therefore, we adopted a new scheme which uses staggered-mesh for E_ρ and Γ_i,Γ_e as illustrated in Fig. 2. Fluxes are evaluated on half-grids $\rho=\rho_{i\pm1/2}$ and time evolution of $E_\rho(\rho_i)$ is calculated as follows

$$\varepsilon_0\varepsilon_\perp\frac{\partial E_\rho(\rho_i)}{\partial t} = -e\left[z_i\bar{\Gamma}_i(\rho_i)-\bar{\Gamma}_e(\rho_i)\right], \tag{9}$$

where $\bar{\Gamma}_i(\rho_i)$ and $\bar{\Gamma}_e(\rho_i)$ are averaged values of those which evaluated at $\rho=\rho_{i\pm1/2}$. With this new scheme, FORTEC-3D can simulate continuous transition from ion-root to electron-root as shown in Fig. 3.

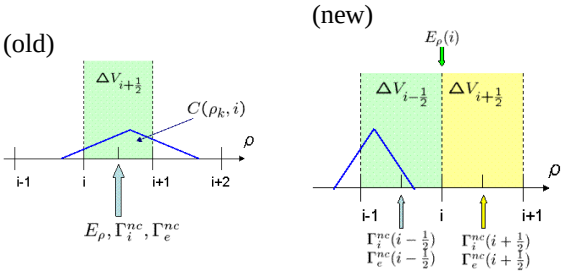

Fig. 2 Radial meshes and positions on which fluxes and electric field are evaluated in old and new schemes.

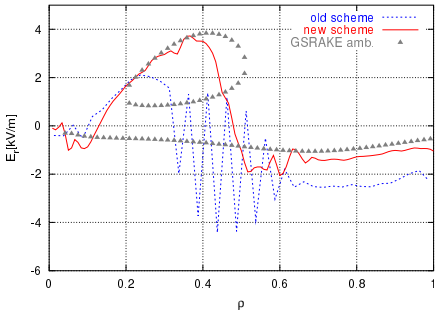

Fig. 3 Comparison of electric field profile between old and new schemes for flux and electric field. Squares are estimation of ambipolar field from GSRAKE.

5 Filtration

Reducing the numerical noise without relying on a massive number of markers is essential to any Monte-Carlo simulation. In the δf method, the origin of big noise is from markers which has huge weights w or p. If collisions and electric potential are neglected, the marker weights can be determined as

$$p_1 = p_0\frac{n_1}{n_0}\left(\frac{T_0}{T_1}\right)^{3/2} e^{\left[-\left(\frac{mv_1^2}{2T_1}\right)^2+\left(\frac{mv_0^2}{2T_0}\right)^2\right]}, \tag{10a}$$

$$w_1 = w_0-(p_1-p_0), \tag{10b}$$

where subscript 0 and 1 represents initial and present values of them at marker position. From eq.(10), it is expected that markers which travels long distance in radial direction will have large marker weights. It is inevitable to appear such large-drift particles in low-collisionality helical plasmas, we need to set limits for weight values. In reality, we found only less than 0.1% of simulation markers have huge weights $p_1\sim|w_1|\gg10p_0$, and these markers makes the calculation very noisy and unstable. Therefore, we apply filters for markers by setting limits for p, $|w|/p$, and v/v_{th}. The second limiter is following from the assumption in δf method that $\delta f/f_M\ll1$, and the third limiter is because fast ions tend to have large orbit widths. The markers which breaks the limits are filtrated out and redistributed around the magnetic axis, which contributes to keep marker population there.

To check the effect of filters, we have carried out several tests with varied strength of filters as shown in Table 1. Note here that the "old" simulation used old $\mathscr{P}$ operator and was not equipped with filters for p. In fig. 4, comparison of radial electric field at three different times with varied filters are shown. As is shown there, the time evolution of E_ρ and quasi-steady state profiles (at the last figure of three) are almost the same regardless of strength of filters. To check the time evolution in detail, we compare E_ρ and Γ_i on $\rho=0.45$ for three filters in Fig. 5. Here, error-bars are evaluated from the variance between every 30 steps. It is found that the filters successfully suppress

the numerical noise even in the weakest filter case, though the start timing of transition differs slightly among three simulations. It is also notable that the simulation marker number can be reduced if we adopt the filters.

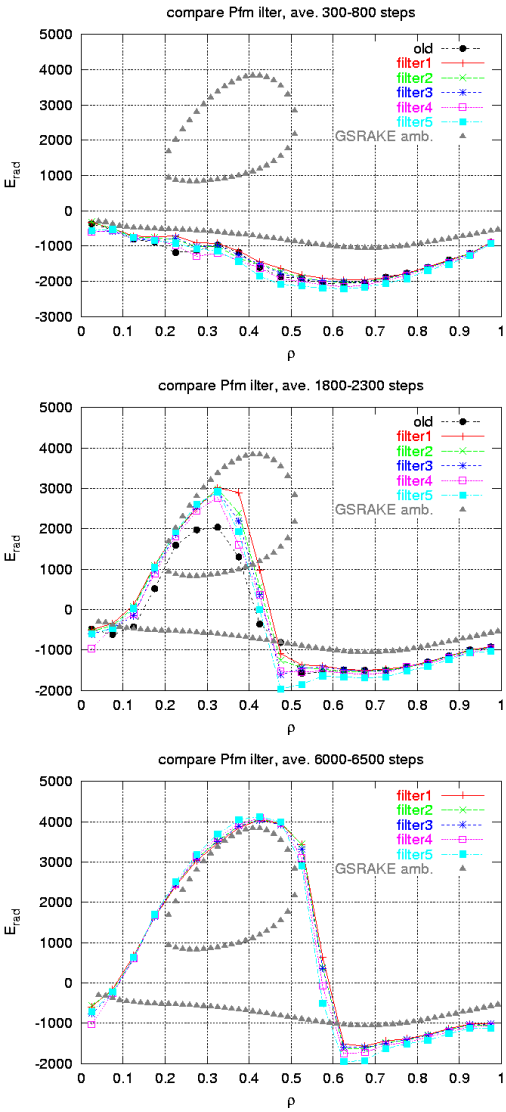

Fig. 4 Comparison of electric field profile between old and new schemes for different filters.

6 Conclusion

The improvements for numerical schemes in FORTEC-3D were proved to reduce numerical errors and noises significantly with little changes in the observable values such as flux and electric field, etc. FORTEC-3D will be applied to study the FOW effects in helical plasmas, bifurcation phenomena, and so on. We are also planning to apply the δf method to solve electron transport and evaluate the bootstrap current in the presence of ambipolar electric field.

[1] D. E. Hastings *et al.*,Nuclear Fusion **25**, 445 (1985).
[2] R. Kanno *et al.*,*et al.*,Nuclear Fusion **37**, 1463 (1997).

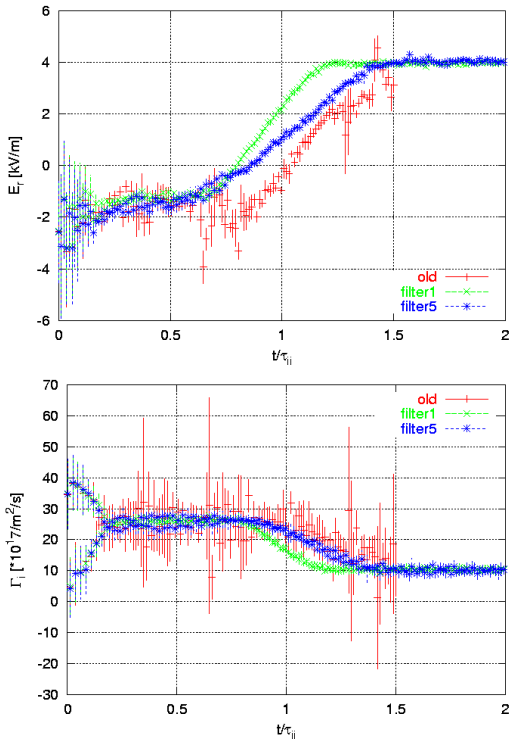

Fig. 5 Comparison of time evolution of E_r and Γ_i between old, filter 1 and filter 5 calculations on $\rho = 0.45$ surface. The oscillation at the beginning phase is GAM.

Table 1 Filter strengths and marker numbers used in test-runs.

	p	$\|w\|/p$	v/v_{th}	marker num.
old	-	2.0	5.0	3.84×10^7
filter 1	5	2.0	4.5	3.84×10^7
filter 2	8	2.5	4.5	3.84×10^7
filter 3	10	2.5	4.5	1.28×10^7
filter 4	25	4.0	4.5	1.92×10^7
filter 5	10	10.0	4.5	1.92×10^7

[3] N. Nakajima *et al.*,J. Phys. Soc. Japan **61**, 833 (1992).
[4] M. Wakatani, *Stellarators and Heliotron Devices* (Oxford Univ. Press, 1998), Chap. 7.
[5] P. Helander, Physics of Plasmas **7**, 2878 (2000).
[6] S. Satake *et al.*,Physics of Plasmas **9**, 3946 (2002) .
[7] S. Satake *et al.*,Plasma Fusion Res. **1**, 002 (2006).
[8] S. Satake *et al.*,Nuclear Fusion **47**, 1258 (2007).
[9] W. X. Wang *et al.*,Plasma Phys. Control. Fusion **41** 1091 (1999).
[10] S. Brunner *et al.*,Physics of Plasmas **6**, 4504 (1999).
[11] W. X. Wang *et al.*,Physics of Plasmas **13** 082501 (2006).
[12] J. L. Lewandowski *et al.*,Physics of Plasmas **8**, 2849 (2001).
[13] M. Yu. Isaev *et al.*,Fusion Science and Technology **50**, 440 (2006).
[14] C. D. Beidler *et al.*,Plasma Phys. Control. Fusion **43**, 1131 (2001).
[15] A. H. Boozer, Phys. Fluids **23**, 904 (1980).
[16] S. P. Hirshman *et al.*,J. Comput. Phys. **96**, 99 (1991).
[17] C. K. Birdsall *et al.*,*Plasma Physics via Computer Simulation* (Inst. Phys. Pub., 1991), Chap. 4.